RSC Advances

PAPER

View Article Online
View Journal | View Issue

Cite this: *RSC Adv.*, 2017, **7**, 7576

Facile synthesis of tea waste/Fe_3O_4 nanoparticle composite for hexavalent chromium removal from aqueous solution

Shisuo Fan,*[ab] Yi Wang,[a] Yang Li,[c] Jun Tang,[a] Zhen Wang,[a] Jie Tang,[a] Xuede Li[ab] and Kai Hu[a]

Received 5th December 2016
Accepted 10th January 2017

DOI: 10.1039/c6ra27781k

www.rsc.org/advances

The modification of biomass waste, as a multifunctional composite, has received tremendous attention for resource utilization and recycling. In this study, tea waste, which is a high level generator of biomass waste, was loaded with nano-Fe_3O_4 particles to prepare a magnetic tea waste/Fe_3O_4 (TW/Fe_3O_4) composite through a facile chemical co-precipitation approach. BET, SEM, TEM, XRD, magnetic properties, FTIR, XPS were used to characterize the TW/Fe_3O_4 composite. A superparamagnetic TW/Fe_3O_4 composite (Fe_3O_4: about 20 nm) was successfully synthesized and possessed the advantages of tea waste and nano-Fe_3O_4 particles. A chromium(VI) adsorption experiment showed that this material has a strong adsorption capacity for aqueous chromium ions, which reached 75.76 mg g^{-1} based on the Langmuir model. The adsorption process could be well fitted by a pseudo-second-order kinetic model and Langmuir, Temkin and Dubinin–Radushkevich (D–R) isotherm models, and was spontaneous and endothermic according to the thermodynamic analysis. The TW/Fe_3O_4 composite revealed good reusability and the removal rate was more than 70% after five recycling cycles. The mechanism of Cr(VI) removal involved electrostatic attraction, reduction process, ion exchange, surface complexation, *etc.* 70% of Cr(VI) was reduced to Cr(III) in this investigation. This study indicated that a TW/Fe_3O_4 composite could be an attractive option for heavy metal treatment.

1. Introduction

Chromium is one of the most worrying pollutants in the environment. The primary sources of chromium include the electroplating, cement, fertilizer, textile and steel industries.[1] The speciation of chromium determines its environmental behavior. The main valences of chromium are Cr(VI) and Cr(III). The mobility and solubility of Cr(VI) are higher in aqueous solution. Cr(VI) may exert a toxic effect on biological systems.[2] Hence, removal of Cr(VI) from the water system is crucial.

Many approaches, including chemical precipitation, ion-exchange, electrochemical, reduction, membrane filtration, and adsorption,[3,4] have been proposed for the removal of Cr(VI) from aqueous solution. Due to the advantages of convenient operation, lower cost, and higher efficiency, the adsorption method has been widely applied. Currently, adsorbents derived from biomass or modified biomass have drawn great attention.[5–8]

With the development of the tea industry, the amount of tea waste has also increased. Tea waste could act as a good absorbent for heavy metal removal from wastewater because of its abundant organic functional groups and cellulose-based pore structure. The removal of metals by tea waste has been reported in previous literature, including Cu^{2+},[9–12] Cd^{2+},[10–12] Zn^{2+},[11,13] Ni^{2+},[13–15] and Pb^{2+}.[9,11–13] Meanwhile, the removal of Cr(VI) by tea waste has also been investigated in previous studies.[16,17]

However, it is difficult to separate powdered adsorbent from an aqueous solution for recycling and the adsorption capacity of biomass for heavy metals is limited. The introduction of magnetic nano-particles into the adsorbent could solve this problem. Chen *et al.*[18] found that loading of Fe_3O_4 nanoparticles into the composite could improve the magnetic and adsorption properties of raw composite. Nano-Fe_3O_4 material had been widely used in wastewater treatment based on its superparamagnetic properties, high surface area, easy separation, lower toxicity, *etc.*[19,20] Meanwhile, the loading of nano-Fe_3O_4 onto a biomass adsorbent could also enhance the dispersibility and stability of nano-Fe_3O_4 particles.[21]

A preliminary investigation into a tea waste/nano particle composite was also carried out. The preparation of a tea waste/nano Fe_3O_4 composite has been used to remove Ni(II) from aqueous solution.[22] Babaev *et al.*[23] investigated Cr(VI) removal by spent tea-supported magnetite nano-particles from aqueous

[a]*School of Resources and Environment, Anhui Agricultural University, Hefei, 230036, P. R. China. E-mail: fanshisuo@ahau.edu.cn; Fax: +86-551-6578-6311; Tel: +86-551-6578-6311*

[b]*Hefei Scientific Observing and Experimental Station of Agro-Environment, Ministry of Agriculture, P. R. China, Hefei, 230036, China*

[c]*College of Environmental Science and Engineering, Tongji University, Shanghai 200092, P. R. China*

solutions. The preparation method was co-precipitation ($FeCl_2 \cdot 4H_2O$ + NaOH) and the maximum adsorption capacity was 30 mg g^{-1}. However, most studies focused on the adsorption thermodynamics or kinetics, and investigation of the adsorption capacity of a tea waste/nano particle composite was limited. The removal of Cr(VI) by tea waste/nano Fe_3O_4 has rarely been reported, especially the adsorption mechanism and potential recycling.

Therefore, tea waste was chosen as the matrix for the synthesis of a composite. Nano-Fe_3O_4 particles were loaded into the tea waste by a chemical co-precipitation method to prepare a magnetic tea waste/Fe_3O_4 composite. The composite was applied to remove Cr(VI) from aqueous solution. The purposes of this study are (1) to investigate the effect of proper parameters, kinetics, and equilibrium on Cr(VI) adsorption on a tea waste/Fe_3O_4 composite; (2) to explore the interaction mechanism between Cr(VI) and the tea waste/Fe_3O_4 composite; (3) to assess the potential recycling of the tea waste/Fe_3O_4 composite acting as Cr(VI) absorbent. Our results showed that a tea waste/Fe_3O_4 composite can be facilely prepared and could be used to remove Cr(VI) from aqueous solution.

2. Materials and methods

2.1. Synthesis of TW/Fe_3O_4 composite

Tea waste was collected from a tea factory in Anhui province, China. The pretreatment procedure of tea waste was described in a previous ref. 22. The chemical co-precipitation method had been used to prepare nano-particles with a homogeneous composition and narrow size distribution.[24] This method was facile and widely used to synthesize nano-particles. The product was called a TW/Fe_3O_4 composite (TW: tea waste) and the reactions are as shown in eqn (1) and (2). To obtain nano-Fe_3O_4 particles, 5.2 g of $FeSO_4 \cdot 7H_2O$ and 7.4 g of $FeCl_3 \cdot 6H_2O$ were put in a three-mouth flask and 80 mL of distilled water was added to dissolve the iron compound with vigorous stirring. When the solution was heated to 80 °C, 20 mL of ammonium hydroxide (25%) was added. Then, 10 g of tea waste was added into the solution and the reaction proceeded for 30 min at 80 °C under constant stirring. The whole process was conducted under the protection of N_2 gas. The reaction product was cooled down to room temperature and then repeatedly washed with distilled water and absolute ethyl alcohol to remove the unreacted chemicals. An external magnet was used to separate the product from the solution. The prepared product was dried in a vacuum oven at 60 °C for 10 h.

$$Fe^{2+} + 2Fe^{3+} + 8OH^- \rightarrow Fe_3O_4 + 4H_2O \quad (1)$$

$$Fe_3O_4 + TW + 4H_2O \rightarrow TW - Fe_3O_4 \quad (2)$$

All the chemicals used were of analytical grade and were purchased from the Sinopharm Group Chemical Reagent Co., Ltd. China. The experiments were determined in triplicate and the average value is shown.

2.2. Batch adsorption experiments

The Cr(VI) stock solution was prepared by dissolving 0.2829 g of $K_2Cr_2O_7$ in 1000 mL of distilled water. The effect of pH, adsorbent dosage, contact time, and temperature on Cr(VI) removal was examined through batch adsorption studies.

An amount of TW/Fe_3O_4 composite (0.04 g) and 40 mL of Cr(VI) solution of 40 mg L^{-1} were mixed in a 50 mL centrifugal tube. The solution pH was adjusted to 2–8 with 0.1 M HCl or 0.1 M NaOH solutions (pH effect). A varying mass of TW/Fe_3O_4 composite and 40 mL of Cr(VI) solution of 25 mg L^{-1} were added to a 50 mL centrifugal tube to give a solid/liquid ratio in the range of 0.1–3 g L^{-1} (dosage effect). The experiment was conducted in an oscillator with the conditions of temperature 298 K, contact time 12 h and an agitation rate of 180 rpm. When the adsorption reached equilibrium, the suspended solution was separated using an external magnet and was passed through a 0.45 μm filter member. The concentration of Cr(VI) in the supernatant was determined by measuring the absorbance of the purple complex of Cr(VI) with 1,5-diphenylcarbazide at 540 nm by a spectrophotometer (722S, Shanghai Precision, Shanghai, China). The removal rate and adsorption amount were calculated according to formulas (3) and (4).

$$R/\% = \frac{C_0 - C_e}{C_0} \times 100\% \quad (3)$$

$$q_e = \frac{C_0 - C_e}{C_0} \times \frac{V}{m} \quad (4)$$

where, C_0 and C_e are the initial and equilibrium concentrations of Cr(VI) (mg L^{-1}), respectively. Herein, q_e is the adsorption amount at equilibrium (mg g^{-1}) and V is the volume of Cr(VI) solution (L); m is the mass of the TW/Fe_3O_4 composite (g).

Adsorption kinetics. The Cr(VI) solution and TW/Fe_3O_4 composite were mixed in a 100 mL Erlenmeyer flask. The pH of the solution was adjusted to 2 using 0.1 M HCl or 0.1 M NaOH solutions. The agitation speed of the oscillator was 180 rpm. The samples were collected at interval times from 0 to 600 min. The adsorption amount was calculated according to formula (5). The kinetic temperature was set at 25 °C, 35 °C and 45 °C. The initial concentrations of Cr(VI) were 10 mg L^{-1}, 30 mg L^{-1}, and 50 mg L^{-1}.

$$q_t = \frac{C_0 - C_t}{C_0} \times \frac{V}{m} \quad (5)$$

where, q_t is the adsorption amount (mg g^{-1}) at time t (min). C_t is the concentration of Cr(VI) at time t (mg L^{-1}).

Adsorption isotherm. An amount of TW/Fe_3O_4 composite (0.04 g) and 40 mL of Cr(VI) solution were mixed in a 50 mL centrifugal tube. The concentration of Cr(VI) solution was set at 10–60 mg L^{-1}. The pH of the solution was adjusted to 2 and the agitation speed of the oscillator was 180 rpm. The contact time was 10 h. The temperature of the isotherm was set at 25 °C, 35 °C and 45 °C.

2.3. Characterization

The textural properties of tea waste and TW/Fe_3O_4 composite were analyzed with a surface area and porosity analyzer (Micromeritics, Tristar II 3020) at 77 K under N_2 atmosphere. The surface area, pore volume and average pore size were calculated using the nitrogen adsorption isotherms. The

multipoint Brunauer–Emmett–Teller method was employed to calculate the surface area. The pore volume and average pore size were obtained from desorption isotherms using the Barrett–Joyner–Halenda method. The surface morphology of the TW/Fe_3O_4 composite was characterized by a Scanning Electron Microscope (SEM, Sirion 200, FEI company, USA) and a Transmission Electron Microscope (TEM, Tecnai G2 spirit Biotwin, FEI, USA). The crystal composition of the TW/Fe_3O_4 composite was also analyzed by X-ray diffraction (XRD, Bruker, D8 Advance, Germany). The magnetic properties of the TW/Fe_3O_4 composite and the adsorbed Cr(VI) composite were determined by a SQUID instrument (MPMS XL-7, Quantum Design, USA). The functional groups of TW/Fe_3O_4 composite and absorbed Cr(VI) composite were measured by Fourier Transform Infrared Spectroscopy (Nicolette is50, Thermo Fourier, USA).

The concentration of released metals (Ca^{2+}, Na^{+}, K^{+}, Mg^{2+}) from the TW/Fe_3O_4 composite in the supernatant of the equilibrium solution was analyzed by inductively coupled plasma optical emission spectroscopy (ICP-OES, PerkinElmer, 2100DV, USA). The corresponding release of Ca^{2+}, Na^{+}, K^{+}, Mg^{2+} from the TW/Fe_3O_4 composite with deionized water served as a control.

The concentration of total Cr in the supernatant was determined by atomic absorption spectroscopy (AAS, ZEEnit 700P, Analytik Jena AG, Germany). The concentration of Cr(VI) was analyzed by spectrophotometer. The concentration of Cr(III) in the supernatant was calculated as the difference between the total Cr and Cr(VI) concentrations.

The valence of the Cr bound on the TW/Fe_3O_4 composite was determined by an X-ray Photoelectron Spectrometer (Thermo-VG Scientific, ESCALAB 250, USA). The Cr-laden TW/Fe_3O_4 composite was obtained by shaking 1 g L^{-1} composite with 50 mg L^{-1} at pH 2 for 10 h.

3. Results and discussion

3.1. Characterization of tea waste/Fe_3O_4 composite

The SEM and TEM spectra of the TW/Fe_3O_4 composite are shown in Fig. 1. The raw tea waste had a fibrous structure due to its cellulose and hemicellulose components (Fig. 1(a)). Fig. 1(b) shows the image of the Fe_3O_4 nano-particles. As shown in Fig. 1(c), the nano-Fe_3O_4 particles had been successfully loaded into the tea waste. The surface and interiors of the tea waste were covered with nano-Fe_3O_4 particles. The introduction of nano-Fe_3O_4 particles increases the pore diameter and provides more adsorption sites to remove Cr(VI). As Fig. 1(d) shows, the TW/Fe_3O_4 composite could be obviously seen and appeared to have a cubic spinel structure. The size of the Fe_3O_4 nano-particles is approximately 20 nm. Thus, the TW/Fe_3O_4 composite had been successfully prepared and was used for the subsequent adsorption experiments.

The XRD spectrum of the TW/Fe_3O_4 composite is shown in Fig. 2. As can be seen in Fig. 2, a Fe_3O_4 crystal compound could be detected and the values of 2θ were 30.20°(220), 35.54°(311), 43.30°(400), 53.50°(422), 57.30°(511), 62.90°(440).[18,25] Thus, nano-Fe_3O_4 particles had been produced and loaded into the tea waste. The peaks (2θ) of the composite which were located nearby at 17° and 22° may relate to the amorphous carbon based on tea waste.

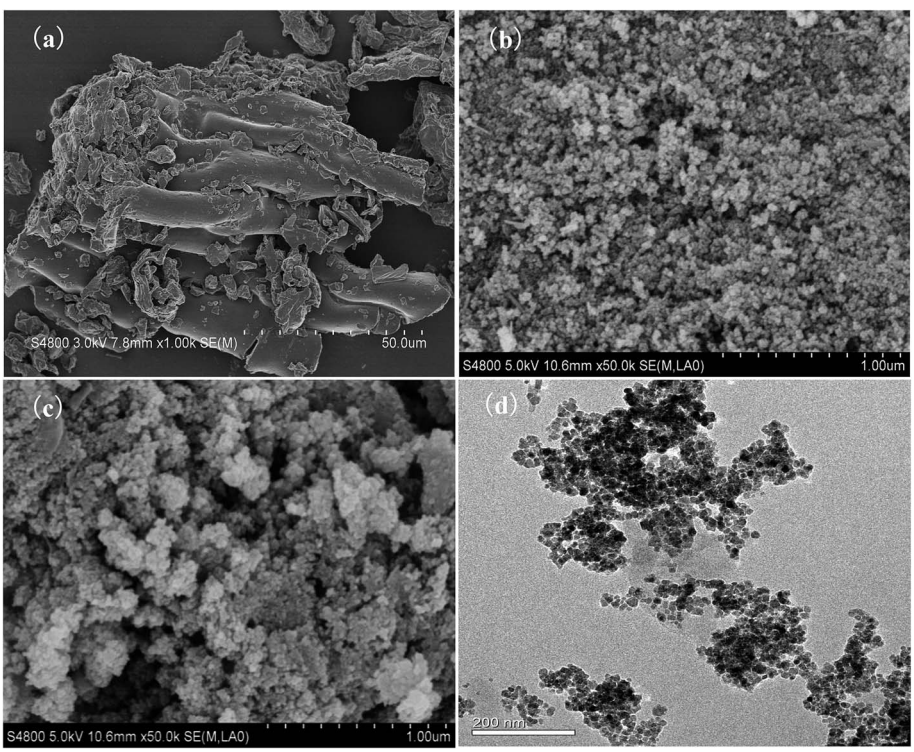

Fig. 1 SEM photo (a) tea waste; (b) Fe_3O_4; (c) TW/Fe_3O_4 composite and (d) TEM of TW/Fe_3O_4 composite.

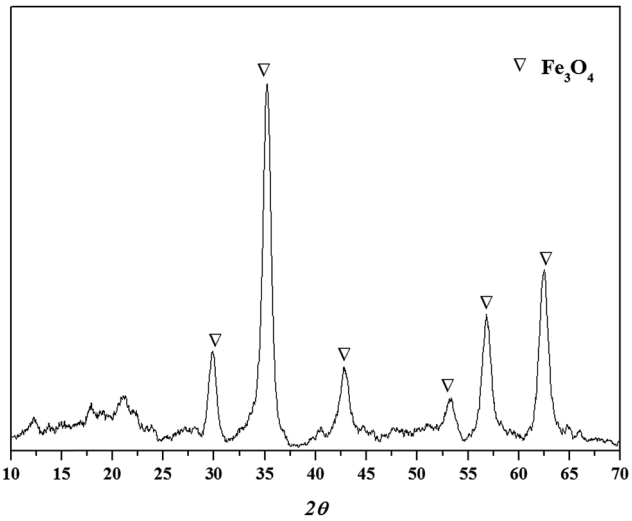

Fig. 2 XRD spectrum of the TW/Fe_3O_4 composite.

The specific surface area, pore volume and average pore diameter of the TW/Fe_3O_4 composite were 6.906 m^2 g^{-1}, 0.042 cm^3 g^{-1} and 65.471 nm, respectively. Meanwhile, the specific surface area, pore volume and average pore diameter of the raw tea waste were 0.913 m^2 g^{-1}, 0.007 cm^3 g^{-1} and 2.611 nm, respectively. Compared with tea waste, the surface area and pore volume of the TW/Fe_3O_4 composite increased significantly. This indicated that more adsorption sites could be provided, benefiting the binding of Cr(VI). However, the average pore diameter of the TW/Fe_3O_4 composite also obviously increased. This means that loading of nano-Fe_3O_4 particles could increase the pore average, consistent with the previous study.[26]

The introduction of nano-Fe_3O_4 particles could cause the composite to be magnetic.

Magnetic hysteresis loops of the TW/Fe_3O_4 composite and the Cr-adsorbed composite are shown in Fig. 3. As shown in the figure, with the increase in magnetic field, the magnetization of the TW/Fe_3O_4 composite also increased and tended to saturation. The saturation magnetization of the TW/Fe_3O_4 composite and adsorbed-Cr composite were 15.8 emu g^{-1} and 16.8 emu g^{-1}, respectively. The TW/Fe_3O_4 composite also showed a good superparamagnetic character though the composite had adsorbed the Cr(VI) aqueous solution. The TW/Fe_3O_4 composite could be easily separated from aqueous solution by an external magnet. Thus, the magnetization curves indicated that the TW/Fe_3O_4 composite possesses a good magnetic characteristic. The magnetic property of the TW/Fe_3O_4 composite also remained after Cr(VI) adsorption, suggesting that the TW/Fe_3O_4 composite has the potential for recycling.

The FTIR spectra of tea waste, Fe_3O_4, TW/Fe_3O_4 and Cr(VI)-adsorbed onto TW/Fe_3O_4 are shown in Fig. 4. The FTIR spectra of tea waste, Fe_3O_4, TW/Fe_3O_4 and Cr(VI) adsorbed onto TW/Fe_3O_4 composite were different and the typical functional groups are presented in Table 1. The peaks of the main functional groups in tea waste include 3416 cm^{-1} (bonded –OH groups), 2924 cm^{-1} and 2852 cm^{-1} (aliphatic C–H group), 1647 cm^{-1} (C=O stretching or aromatic C=C and C=O/C=C stretching), 1536 cm^{-1} (secondary amine group), 1452 cm^{-1} (C–H alkanes in aromatic rings), 1370 cm^{-1} (C–H bending $-CH_3$ symmetric bending of CH_3), 1234 cm^{-1} ($-SO_3$ stretching/P=O), 1149 cm^{-1} (C–O–C of polysaccharides), 1036 cm^{-1} (C–O–H stretching), 613 cm^{-1} (–C–C–).[27,28] Thus, tea waste contains protein-like, aliphatic-like, cellulose-like substances which have hydroxyl, carboxyl, and amine groups, and S- and P-containing functional groups. The obvious peak at 583 cm^{-1} in the spectrum of Fe_3O_4 indicates Fe–O, suggesting the assignment of Fe_3O_4. Other peaks were at 892 cm^{-1} (Fe–O–H), 1630 cm^{-1} and 1400 cm^{-1} (hydroxyl groups from water adsorbed during the preparation of the TW/Fe_3O_4 composite).[29,30] The peaks of the main functional groups of the TW/Fe_3O_4 composite include 3423 cm^{-1} (bonded –OH groups), 2923 cm^{-1} and 2852 cm^{-1} (aliphatic C–H group), 1630 cm^{-1} (assigned to C=O and C=C aromatic vibrations), 1518 cm^{-1} (secondary amine group), 1367 cm^{-1} (C–O stretching vibration), 1215 cm^{-1} (C–N stretching), 1151 cm^{-1} (C–O stretching of ether

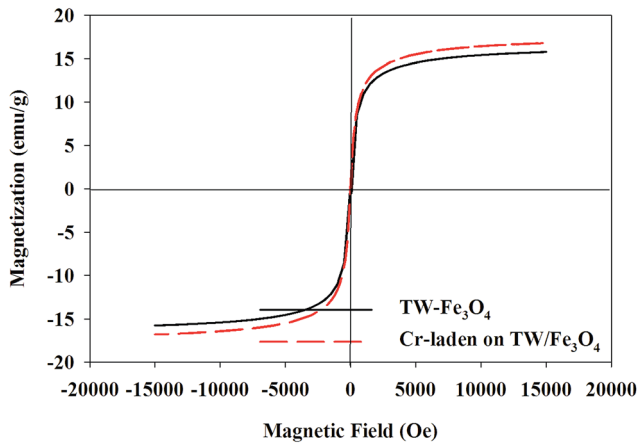

Fig. 3 Magnetic hysteresis loops of the TW/Fe_3O_4 composite and Cr(VI) laden on the composite.

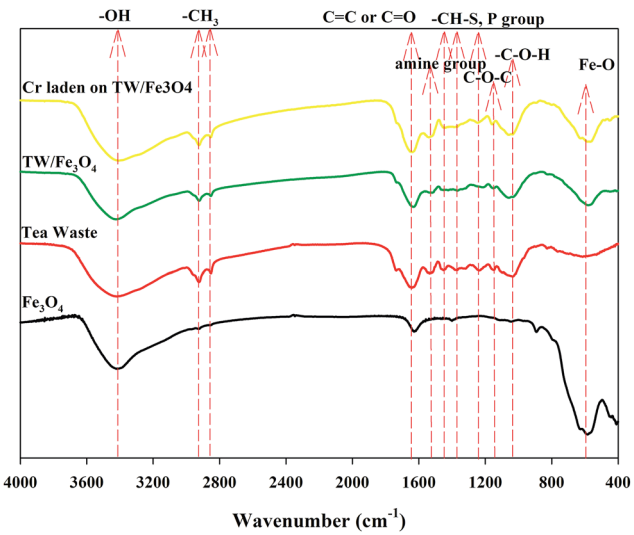

Fig. 4 The FTIR spectrum of tea waste, Fe_3O_4, TW/Fe_3O_4 and Cr laden on the TW/Fe_3O_4 composite.

Table 1 FTIR spectral characteristics of the TW/Fe_3O_4 composite before and after Cr(VI) adsorption

				TW/Fe_3O_4			
Tea waste cm^{-1}	Assignment	Fe_3O_4 cm^{-1}	Assignment	Before adsorption	After adsorption	Difference	Assignment
3416	Bonded –OH groups	3423	Hydroxyl groups	3423	3406	+17	Bonded –OH groups
2924	Aliphatic C–H group	1630	Hydroxyl groups	2923	2923	0	Aliphatic C–H group
2852	Aliphatic C–H group	1400	Hydroxyl groups	2852	2852	0	Aliphatic C–H group
1647	C=O stretching aromatic C=C C=O/C=C stretching	892	Fe–O–H	1630	1640	−10	Assigned to C=O and C=C aromatic vibrations
1536	Secondary amine group	583	Fe–O	1518	1541	−23	Secondary amine group
1452	C–H alkanes in aromatic rings			1367	1385	−18	C–O stretching vibration
1370	C–H bending $–CH_3$ symmetric bending of CH_3			1215	1246	−31	C–N stretching
1234	$–SO_3$ stretching/P=O			1151	1158	0	C–O stretching of ether groups
1149	C–O–C of polysaccharides			1059	1059	0	C–O stretching of COOH
1036	C–O–H stretching			579	579	0	Fe–O
613	–C–C–						

groups), 1059 cm^{-1} (C–O stretching of COOH), 579 cm^{-1} (Fe–O). Thus, the TW/Fe_3O_4 composite retained the functional groups of tea waste and also loaded the functional groups of nano-Fe_3O_4. Meanwhile, the introduction of Fe_3O_4 also changed some functional groups of tea waste and led to a shift in some peaks or the intensity reduction of some peaks, such as 1647 cm^{-1}, 1536 cm^{-1}, 1452 cm^{-1}, 1234 cm^{-1}, and 1036 cm^{-1}.

When the Cr(VI) was adsorbed on the TW/Fe_3O_4 composite, some peaks had changed, including 3423 → 3406 cm^{-1}, 1630 → 1640 cm^{-1}, 1518 → 1541 cm^{-1}, 1367 → 1385 cm^{-1}, 1215 → 1246 cm^{-1}. Hence, –OH, C=O and C=C, C–O, the secondary amine groups, and C–N functional group may participate in the adsorption of Cr(VI), referring to surface complexation, ion exchange, *etc.*

The XPS spectrum of the TW/Fe_3O_4 composite and Cr(VI) adsorbed onto TW/Fe_3O_4 are displayed in Fig. 5. As shown in Fig. 5(a), elements in the TW/Fe_3O_4 composite involve C, O, Fe, *etc.* When the Cr(VI) was adsorbed on the TW/Fe_3O_4 composite, the Cr was detected (as shown in Fig. 5(b)). The fitting of the Cr valence is shown in Fig. 5(c).

The binding energies at 587.2 and 576.9 eV could be assigned to Cr(III) and binding energies at 578.2 and 580.9 eV could be attributed to Cr(VI).[31–37] The ratio of Cr(III)/Cr(VI) was 1.68, based on the peak area analysis. The results confirm that both Cr(VI) and Cr(III) coexist on the surface of the Cr(VI)-adsorbed TW/Fe_3O_4 composite. Thus, most of the Cr bound to the adsorbent was in the trivalent state during Cr(VI) adsorption. The results of XPS confirm that the reduction of Cr(VI) to Cr(III) by the TW/Fe_3O_4 composite is the major process, while more Cr(VI) was bound in a reduced state of Cr(III) during the process.

When the Cr(VI) was reduced to Cr(III), organic compounds in tea waste were responsible for reducing Cr(VI), including carboxyl, methoxy, carbonyl, and hydroxyl groups, and amino groups which could act as electron-donors. Meanwhile, under the acidic atmosphere, few Fe^{2+} ions may be oxidized by Cr(VI), although Fe_3O_4 nanoparticles are relatively stable and further confirmation is needed in future research.

3.2. Effect of pH

pH is a key factor in the adsorption process and affects the surface charge of the adsorbent, the degree of ionization, and the speciation of metals in the solution.[38]

The adsorption of Cr(VI) on the TW/Fe_3O_4 composite is highly pH dependent. The effect of pH on the adsorption of Cr(VI) onto the TW/Fe_3O_4 composite was investigated in the pH range from 2 to 8. As shown in Fig. 6(a), pH significantly affects Cr(VI) removal. With an increase in pH, the removal rate of Cr(VI) significantly decreased. When the pH was 2, the removal of Cr(VI) was more than 90%. When the pH was 3, the removal of Cr(VI) was lower than 50%. The removal of Cr(VI) decreased when the pH was larger than 3. Thus, pH 2 was a suitable parameter in this work. All subsequent adsorption experiments herein were conducted at pH 2, the optimum pH for adsorption of Cr(VI) onto the TW/Fe_3O_4 composite.

pH influenced the surface charge and the protonation degree of the TW/Fe_3O_4 composite. The main Cr(VI) species are $HCrO_4^-$, CrO_4^{2-}, $Cr_2O_7^{2-}$, *etc.*[39,40] When the pH was lower, the surface charge of the TW/Fe_3O_4 composite caused a protonation reaction and more positive charge formed. The binding site of the TW/Fe_3O_4 composite could interact with Cr(VI) through electrostatic attraction or an ion exchange process. With the increase in pH, OH^- increased and competed with $HCrO_4^-$, leading to a decrease in Cr(VI) removal efficiency.[41] Meanwhile, the positive surface charge of Fe_3O_4 could attract $HCrO_4^-$ through electrostatic interaction under the acidic conditions, consistent with previous studies.[42,43]

3.3. Effect of TW/Fe_3O_4 composite dosage

Adsorbent dosage is also an important parameter to determine its adsorption ability. The effect of dosage on removal rate and adsorption amount is shown in Fig. 6(b). As shown in Fig. 6(b), as the dosage was increased from to 0.1 to 1, the removal rate of Cr(VI) increased from 20% to 90%. When the adsorbent dosage

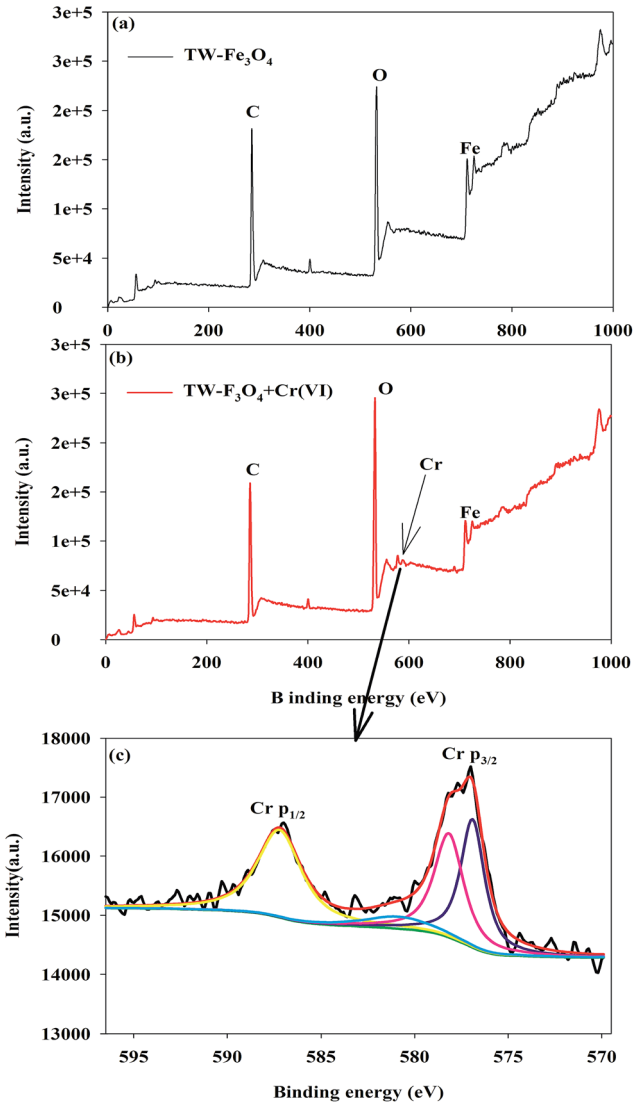

Fig. 5 XPS analysis of the TW/Fe_3O_4 composite and absorbed Cr on the TW/Fe_3O_4 composite (a) TW/Fe_3O_4 composite (b) Cr laden on the TW/Fe_3O_4 composite (c) speciation analysis of Cr.

was larger than 1, the removal rate increased slightly, suggesting that the adsorption reached a saturated state. The TW/Fe_3O_4 composite provided enough adsorption sites to bind the Cr(VI). However, adsorption density (adsorption capacity for unit mass of the adsorbent) decreased with an increase in adsorbent concentration due to formula (3). This was consistent with the previous study.[44] After comprehensive consideration of removal rate, adsorption capacity, and cost, the optimum absorbent dosage was found to be 1 g L^{-1}.

3.4. Effect of contact time, initial concentration and temperature on the removal of Cr(VI)

The contact time, initial concentration and temperature also had pronounced effects on the removal of Cr(VI) from aqueous solution. The effects of these parameters on Cr(VI) removal rate are shown in Fig. 7. The rate of Cr(VI) uptake was quite fast for the first 30 min. The adsorption reaction reached equilibrium when the contact time was 10 h.

When the initial concentration of Cr(VI) was higher, the rate of Cr(VI) removal was relatively slow at the beginning. With a prolonged contact time, the adsorption ultimately reached equilibrium. The removal rate was higher when the initial concentration of Cr(VI) was lower under the same conditions, as the TW/Fe_3O_4 composite could provide more adsorption sites. When the initial concentration of Cr(VI) was the same, a higher temperature led to a higher removal rate in the temperature range of 25–45 °C. A higher temperature was beneficial for the adsorption of Cr(VI) on the TW/Fe_3O_4 composite.

3.5. Adsorption kinetics

Based on the adsorption kinetics of Cr(VI) onto the TW/Fe_3O_4 composite, experimental data was fitted using pseudo-first-order, pseudo-second-order, intra-particle diffusion and Elovich models.[45–48] The kinetic equations are expressed as the following eqn (6)–(9).

Pseudo-first-order

$$\log(q_e - q_t) = \log q_e - \frac{k_1}{2.303} t \quad (6)$$

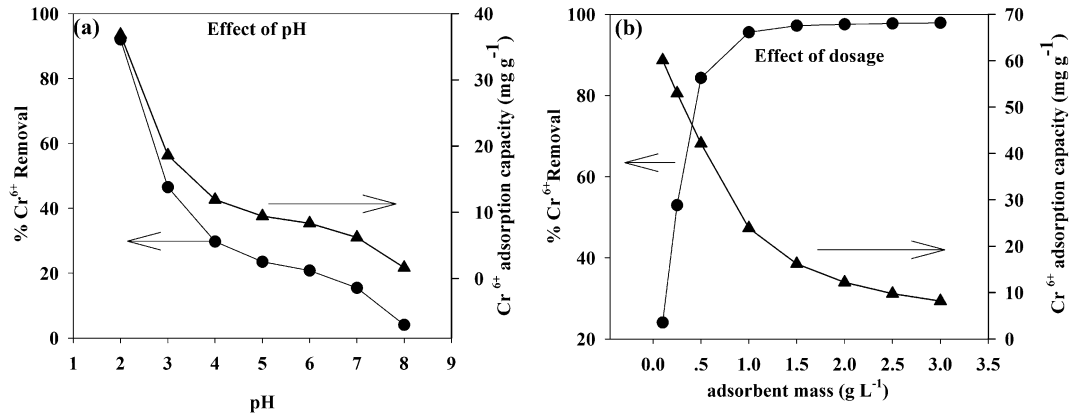

Fig. 6 Effect of (a) pH and (b) adsorbent mass on Cr(VI) removal.

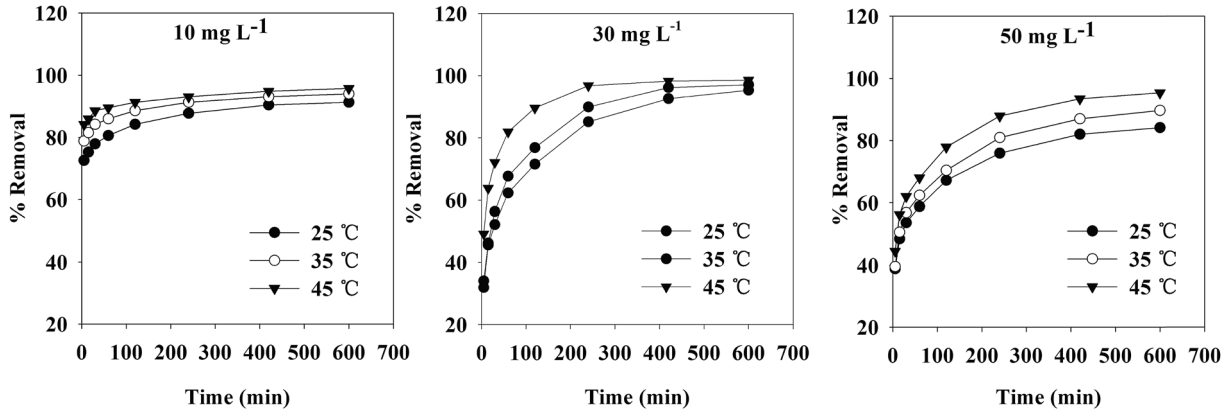

Fig. 7 Effect of contact time, initial concentration and temperature on Cr(VI) adsorption.

Pseudo-second-order

$$\frac{t}{q_t} = \frac{1}{k_2 q_e^2} + \frac{t}{q_e} \quad (7)$$

Intra-particle diffusion

$$q_t = k_{id} t^{1/2} + C \quad (8)$$

Evolich

$$q_t = (1/\beta)\ln(\alpha\beta) + 1/\beta \ln(t) \quad (9)$$

where, q_t and q_e (mg g^{-1}) are the adsorption capacities of Cr(VI) ions at time t and equilibrium time, respectively. k_1 (min^{-1}) and k_2 (g mg^{-1} min^{-1}) are the pseudo-first-order and pseudo-second-order rate constants, respectively. k_{id} (mg g^{-1} $min^{-0.5}$) is the intra-particle diffusion rate constant and C is the intercept (mg g^{-1}) and its value stands for the thickness of the boundary layer. α is the initial adsorption coefficient (mg g^{-1} min^{-1}) and β is the desorption coefficient (g mg^{-1}).

The kinetic fitting of Cr(VI) on the TW/Fe_3O_4 composite at 298 K is shown in Fig. 8.

The fitting parameters of pseudo-first-order and pseudo-second-order kinetics are presented in Table 2. The

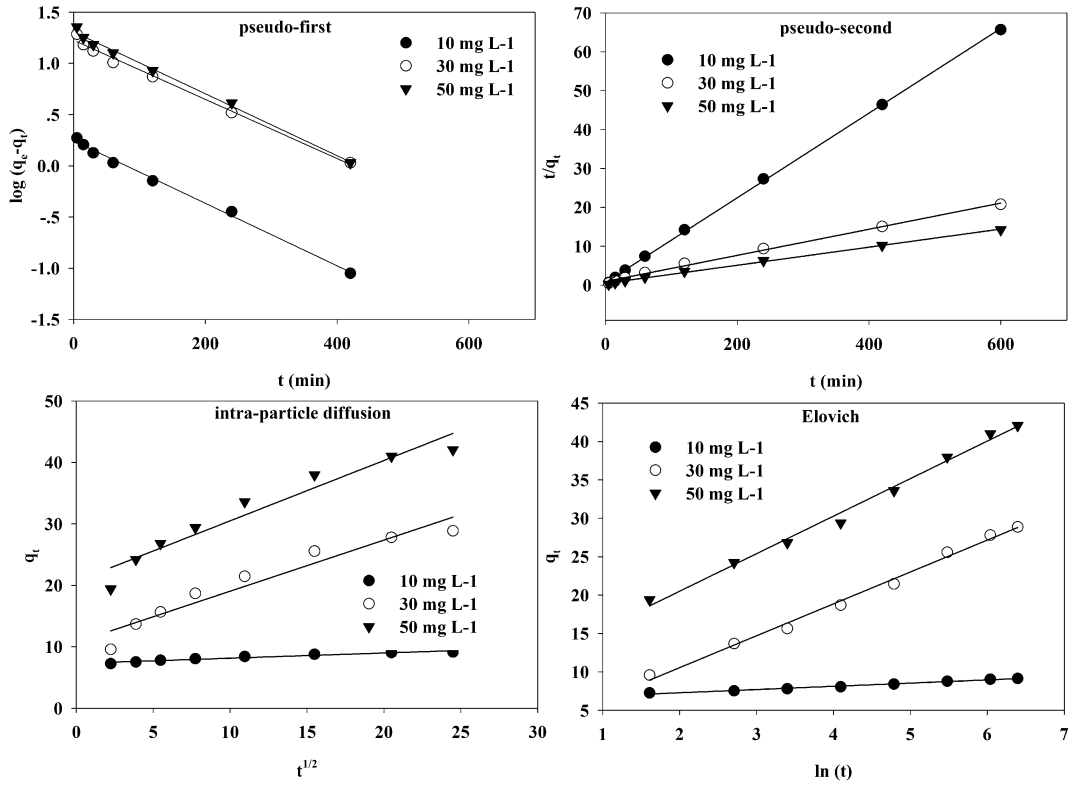

Fig. 8 Pseudo-first-order, pseudo-second-order, intra-particle diffusion, and Elovich kinetics models of Cr(VI) adsorption onto the TW/Fe_3O_4 composite at 298 K.

Table 2 Parameters of kinetic models for adsorption of Cr(VI) onto the TW/Fe_3O_4 composite (pseudo-first-order and pseudo-second-order kinetics models)

Initial concentration (mg L^{-1})	T (K)	Pseudo-first-order			Pseudo-second-order		
		q_e	k_1	R^2	q_e	k_2	R^2
10	298	1.7557	0.0070	0.9945	9.1827	0.0175	0.9997
	308	1.3006	0.0065	0.9863	9.3897	0.0243	0.9998
	318	0.9838	0.0057	0.9758	9.5923	0.0302	0.9999
30	298	16.8601	0.0069	0.9915	29.7530	0.0012	0.9964
	308	17.1712	0.0083	0.9940	30.3674	0.0014	0.9982
	318	11.9989	0.0120	0.9897	30.1023	0.0033	0.9998
50	298	20.3470	0.0070	0.9934	42.9738	0.0012	0.9976
	308	21.9149	0.0067	0.9921	45.7875	0.0010	0.9974
	318	22.4647	0.0075	0.9944	48.7329	0.0011	0.9983

correlation coefficient (R^2) was larger than 0.99 and indicates that pseudo-first-order and pseudo-second-order kinetic models could fit the adsorption process well. However, the calculated q_e from the pseudo-first-order kinetic model shows a large difference from the q_e from experiment. The calculated q_e from the pseudo-second-order kinetic model was close to the q_e from experiment. Thus, the pseudo-second-order model could better fit the adsorption process of Cr(VI) onto the TW/Fe_3O_4 composite. Generally, the pseudo-second-order kinetic model was used to describe chemisorption, referring to valency force through the sharing or exchange of electrons between the adsorbent and adsorbate as covalent forces, and ion exchange.[46,49,50] Therefore, the removal rate of Cr(VI) by the TW/Fe_3O_4 composite was controlled by a chemisorption mechanism.

The fitting parameters of the intra-particle diffusion and Evolich models are shown in Table 3. Intra-particle diffusion is a transport process which describes the movement of species from the bulk of the solution to the solid phase.[45] The correlation coefficient (R^2) was larger than 0.90, indicating that intra-particle kinetic models could also fit the adsorption process. The line does not pass through the origin, which means that the adsorption of Cr(VI) onto the TW/Fe_3O_4 composite was controlled by chemisorption coupled with intra-particle diffusion, involving electron sharing or electron transfer.[47]

The Elovich kinetic equation is used to interpret the kinetics of chemisorption on highly heterogeneous sorbents.[51] The correlation coefficient (R^2) was larger than 0.95, indicating that the Evolich model could also fit the adsorption process well. Chemisorption plays an important role during the adsorption of Cr(VI) onto the TW/Fe_3O_4 composite.

Herein, the focus of our research is the adsorption process of the Cr(VI) on the TW/Fe_3O_4 composite. The reduction of Cr(VI) is the subsequent reaction after the Cr(VI) reaches the surface of the TW/Fe_3O_4 composite. The reduction process may influence the isotherm/kinetics models and belongs to the whole adsorption process. Recently, advanced reduction kinetics have been developed to fit the kinetics process and confirmed the "reduction mechanism".[52,53] Further research is needed in the future.

3.6. Adsorption isotherms

The equilibrium adsorption isotherm is fundamental in describing the interactive behavior between adsorbates and adsorbent, and is important in the design of adsorption systems.[54–57] Research into adsorption isotherms is crucially important in the modeling, design, and commercial application of adsorbents.[58–60]

The Langmuir, Freundlich, Temkin and Dubinin–Radushkevich (D–R) isotherms were expressed as the following eqn (10)–(15).

Langmuir:

$$\frac{C_e}{q_e} = \frac{1}{q_{max} K_L} + \frac{C_e}{q_{max}} \quad (10)$$

Table 3 Parameters of kinetic models for the adsorption of Cr(VI) onto a TW/Fe_3O_4 composite (intra-particle and Evolich kinetics models)

Initial concentration (mg L^{-1})	T (K)	Intra-particle model			Evolich model		
		k_d	C	R^2	α	β	R^2
10	298	0.0840	7.2950	0.9430	2.4696×10^6	2.4155	0.9910
	308	0.8310	10.7200	0.9320	7.1403×10^0	0.2410	0.9930
	318	0.9810	20.6700	0.9360	4.3934×10^1	0.2047	0.9910
30	298	0.0650	7.9780	0.9220	1.5283×10^9	3.0488	0.9960
	308	0.8360	11.7100	0.9000	8.3477×10^0	0.2355	0.9940
	318	1.0720	21.4100	0.9320	3.7918×10^1	0.1868	0.9930
50	298	0.0490	8.4870	0.9280	3.4964×10^{13}	4.0816	0.9820
	308	0.5990	7.5900	0.7900	8.5280×10^1	0.3114	0.9710
	318	1.0950	24.1700	0.9190	5.6834×10^1	0.1817	0.9930

Freundlich:

$$\ln(q_e) = \ln(K_F) + \frac{1}{n}\ln(C_e) \quad (11)$$

Temkin:

$$q_e = \frac{RT}{b_T}\ln(K_T) + \frac{RT}{b_T}\ln(C_e) \quad (12)$$

Dubinin–Radushkevich (D–R) equation:

$$\ln(q_e) = \ln(q_m) - \beta_{D-R}\varepsilon^2 \quad (13)$$

$$\varepsilon = RT\ln\left(1 + \frac{1}{C_e}\right) \quad (14)$$

$$E_a = \frac{1}{\sqrt{2\beta_{D-R}}} \quad (15)$$

where C_e is the equilibrium concentration, mg L^{-1}; q_e is the adsorption capacity at equilibrium time, mg g^{-1}; b is the Langmuir constant, L g^{-1}; q_{max} is the maximum adsorption capacity, mg g^{-1}; K_f is the Freundlich constant, L mg^{-1}; $1/n$ is the heterogeneity of the sorption sites and is an indicator of isotherm nonlinearity; K_T is the equilibrium binding constant, L mg^{-1}; b_T is the Temkin isotherm constant; RT/b_T is related to adsorption heat, J mol^{-1}. q_m is the theoretical isotherm saturation capacity (mol g^{-1}); β_{D-R} is the Dubinin–Radushkevich isotherm constant (mol^2 kJ^{-2}), ε is the Dubinin–Radushkevich isotherm constant.

The fitting curves of the different isotherm equations are displayed in Fig. 9.

The adsorption isotherms and fitting results are shown in Table 4. According to the correlation coefficient, Langmuir, Temkin and D–R isotherms could fit the adsorption process well. The maximum adsorption capacity of Cr(VI) by the TW/Fe_3O_4 composite was 75.76 mg g^{-1}. The maximum adsorption capacity of the TW/Fe_3O_4 composite is much higher than that of most adsorbents reported in the literature,[5] and thus it can be applied as a highly efficient adsorbent to remove trace Cr(VI) from aqueous solution. The Langmuir constant (b) was in the range of 0–1, indicating that the TW/Fe_3O_4 composite had a good potential to remove Cr(VI). Thus, the adsorption of Cr(VI) onto the TW/Fe_3O_4 composite related to monomolecular adsorption. With the increase in temperature, the maximum adsorption capacity gradually increased, suggesting that higher temperatures benefit the adsorption process.

A dimensionless separation factor R_L was defined as $R_L = 1/(1 + C_0b)$.[61] The value of R_L indicates the shape of the isotherm to be either unfavourable ($R_L > 1$), linear ($R_L = 1$), favourable ($0 < R_L < 1$) or irreversible ($R_L = 0$).[62,63] As shown in Fig. 10, R_L was lower than 1 in this study and the adsorption was favorable. A higher initial concentration and temperature benefited the adsorption of Cr(VI) onto the TW/Fe_3O_4 composite.

The Temkin isotherm model assumes that the heat of adsorption decreases linearly rather than logarithmically with coverage and describes the chemisorption interaction with primarily electrostatic interactions. In this study, the correlation coefficient of the Temkin model was larger than 0.95. Thus,

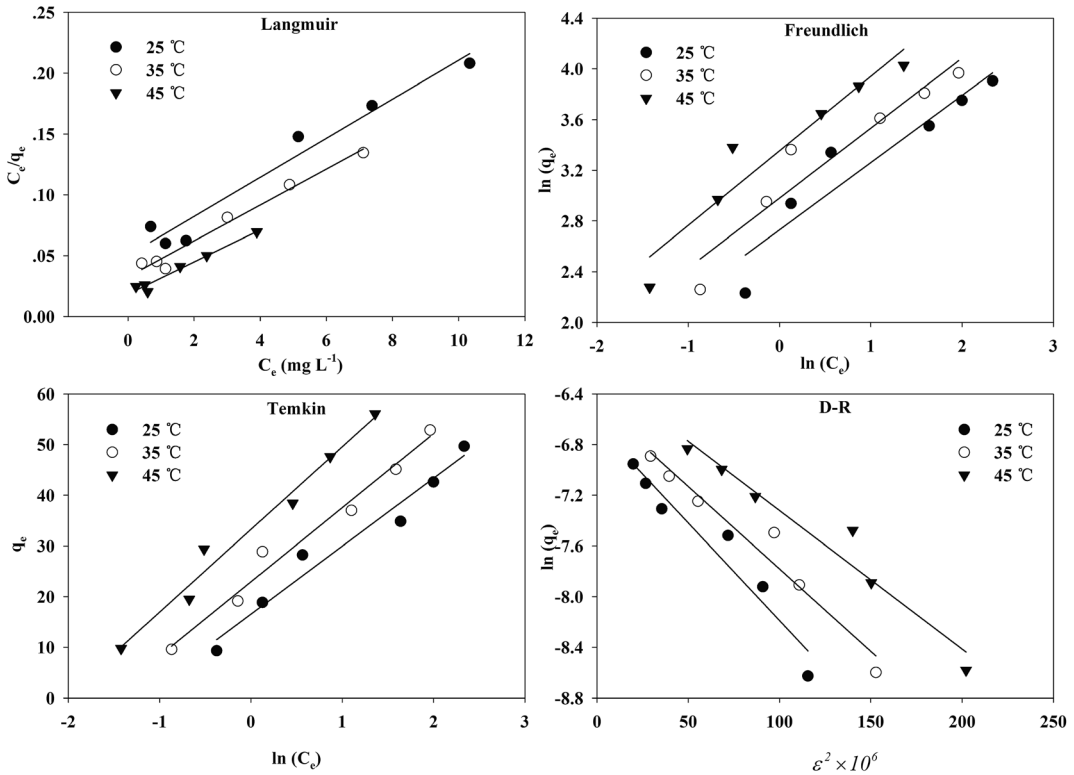

Fig. 9 The fitting of Langmuir, Freundlich, Temkin, D–R isotherms for Cr(VI) adsorption onto the TW/Fe_3O_4 composite.

Table 4 Isotherm parameters for the adsorption of Cr(VI) onto a TW/Fe_3O_4 composite at various temperatures

	Langmuir			Freundlich		
Temperature (°C)	q_{max}	b	R^2	K_f	n	R^2
25	62.11	0.3214	0.9609	15.3375	1.8854	0.8876
35	67.57	0.4554	0.9786	19.6957	1.8096	0.9150
45	75.76	0.7174	0.9720	28.6141	1.7010	0.9132

	Temkin			D–R			
Temperature (°C)	A	B	R^2	q_m	β	E	R^2
25	3.4305	13.4120	0.9647	3.14541×10^{-5}	0.0150	8.1650	0.9330
35	4.7987	14.6180	0.9795	3.6362×10^{-5}	0.0130	8.7706	0.9580
45	7.6963	16.2970	0.9776	5.2102×10^{-5}	0.0100	10.000	0.9500

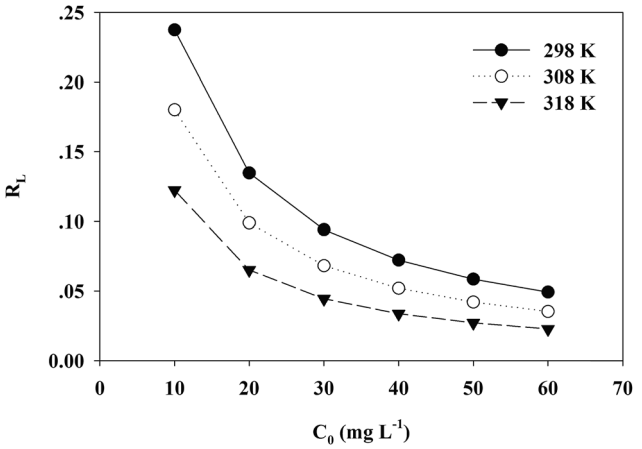

Fig. 10 The variation of R_L under different initial concentrations and temperatures.

electrostatic interaction was an important mechanism between Cr(VI) and the TW/Fe_3O_4 composite, consistent with the result of the pH effect.

The D–R isotherm could also well describe the adsorption process of Cr(VI) onto the TW/Fe_3O_4 composite. When E_a is in the range of 1–8 kJ mol^{-1}, physical interaction plays an important role. When E_a is between 8 and 16 kJ mol^{-1}, the main interaction is an ion exchange process. Chemisorption interaction was the main mechanism when E_a ranged from 16 to 40 kJ mol^{-1}.[64] In this research, E_a ranged from 8 to 10 kJ mol^{-1} when the temperature was between 25 and 45 °C. The fitting results showed that the main adsorption mechanism was ion exchange between Cr(VI) and the TW/Fe_3O_4 composite, coexisting with physical interaction. With an increase in temperature, the increased E_a suggests that the chemisorption interaction became more pronounced.

3.7. Adsorption thermodynamics

In order to better understand the effect of temperature on the adsorption of Cr(VI) on the TW/Fe_3O_4 composite, the thermodynamic parameters of the adsorption process such as change in standard free energy (ΔG), enthalpy (ΔH), and entropy (ΔS) can be calculated using the eqn (16)–(18).[65,66]

$$K_0 = \frac{q_e}{C_e} \tag{16}$$

$$\Delta G = -RT \ln(K_0) \tag{17}$$

$$\ln K_0 = \frac{\Delta S}{R} - \frac{\Delta H}{R}\frac{1}{T} \tag{18}$$

where K_0 is the apparent equilibrium constant. R is the ideal gas constant (4.187 J mol^{-1} K^{-1}) and T is Kelvin temperature (K).

According to the method suggested by Khan and Singh,[66] the sorption distribution coefficient K_0 for the sorption reaction was determined from the slope of the plot $\ln(q_e/C_e)$ against C_e at various temperatures and extrapolating to zero C_e. The values of ΔH and ΔS can be obtained from the slope and intercept of a plot of $\ln K_0$ against $1/T$ and are shown in Fig. 11.

The thermodynamic parameters of Cr(VI) adsorption on the TW/Fe_3O_4 composite are given in Table 5. The ΔG value was negative for all three considered temperatures, and this

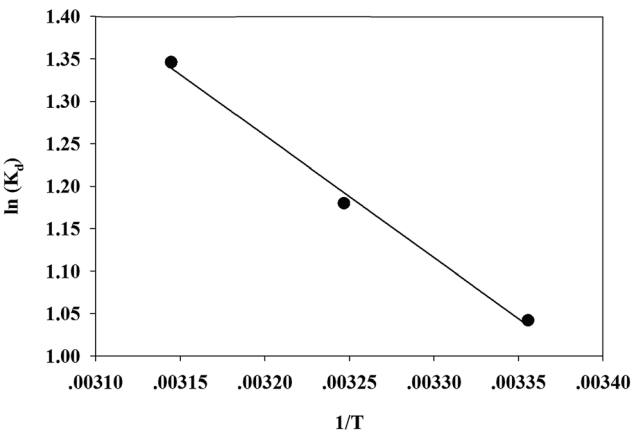

Fig. 11 Plotting of ln(K_d) against 1/T.

Table 5 Parameters of thermodynamic models for the adsorption of Cr(VI) onto a TW/Fe_3O_4 composite

Temperature (K)	ΔG (kJ mol^{-1})	ΔH (kJ mol^{-1})	ΔS (J mol^{-1} K^{-1})
298	−2.5817	11.964	48.770
308	−3.0214		
318	−3.5593		

suggests that the adsorption was a spontaneous process. As the temperature increases, the ΔG values decrease, indicating that elevated temperatures benefit the adsorption process. The ΔH value was positive and the adsorption process was endothermic. The positive value of ΔS confirms that the randomness of Cr(VI) increased at the solid–solution interface during the adsorption process.

3.8. Concentration of different Cr species under different parameters

The concentrations of different Cr species under various parameters are shown in Fig. 12. It was found that the concentrations of total and hexavalent chromium were not equal, which meant that after the contact between the TW/Fe_3O_4 composite and Cr(VI) solutions, the Cr(III) concentration rose in solution. This result also confirmed that a chemical redox reaction occurs during the adsorption process.

As shown in Fig. 8(a), when the pH was lower than 4, Cr(III) could be detected in the solution. This indicated that Cr(VI) was easily reduced to Cr(III) under acidic conditions. The experimental result was in line with the effect of pH on Cr(VI) removal.

The effect of adsorbent dosage is presented in Fig. 8(b). The experimental conditions were consistent with the effect of dosage on Cr(VI) removal. When the solid–liquid ratio was larger than 0.25, the reduction reaction occurred under acidic conditions. When the solid–liquid ratio was larger than 1, the concentration remained stable because the Cr(VI) was adsorbed onto the TW/Fe_3O_4 composite and was reduced to Cr(III). Cr(VI) could not be detected in the solution.

The effect of contact time is described in Fig. 8(c). The experimental conditions were equal to those of the adsorption kinetics (initial concentration of Cr(VI) was 50 mg L^{-1}). Cr(III) could be detected in the solution of the adsorption experiment after 5 min. The concentration of Cr(III) increased as the contact time increased. When Cr(VI) was reduced to Cr(III) on the surface of the TW/Fe_3O_4 composite, part of the Cr(III) was released into solution due to electrostatic repulsion.[67]

The proportion of reduced Cr was calculated by means of XPS analysis and the results of Fig. 8(c) using formula (19). The results showed that 70% of Cr(VI) was reduced to Cr(III). 30% of the Cr(VI) was adsorbed onto the surface of the TW/Fe_3O_4 and existed in solution.

$$\text{Reduction } (\%) = \frac{\text{Cr(III)}_{\text{solution}} V + \frac{1.68}{2.68}\{C_0 V - [\text{Cr(VI)}_{\text{solution}} + \text{Cr(III)}_{\text{solution}}] V\}}{C_0 V} \times 100 \quad (19)$$

where, reduction (%) is the reduction ratio of Cr(VI). Cr(III)$_{\text{solution}}$, Cr(VI)$_{\text{solution}}$ are the concentration of Cr(III), Cr(VI) in solution when the adsorption reached equilibrium (mg L^{-1}). C_0 is the initial concentration of Cr(VI). V is the volume of Cr(VI) solution (L) 1.68/2.68 is the ratio of Cr(III)/[Cr(VI) + Cr(III)] based on the peak area analysis of XPS.

3.9. Desorption and regeneration experiment

Desorption and regeneration batch experiments were designed to study the recoverable potential of the TW/Fe_3O_4 composite.

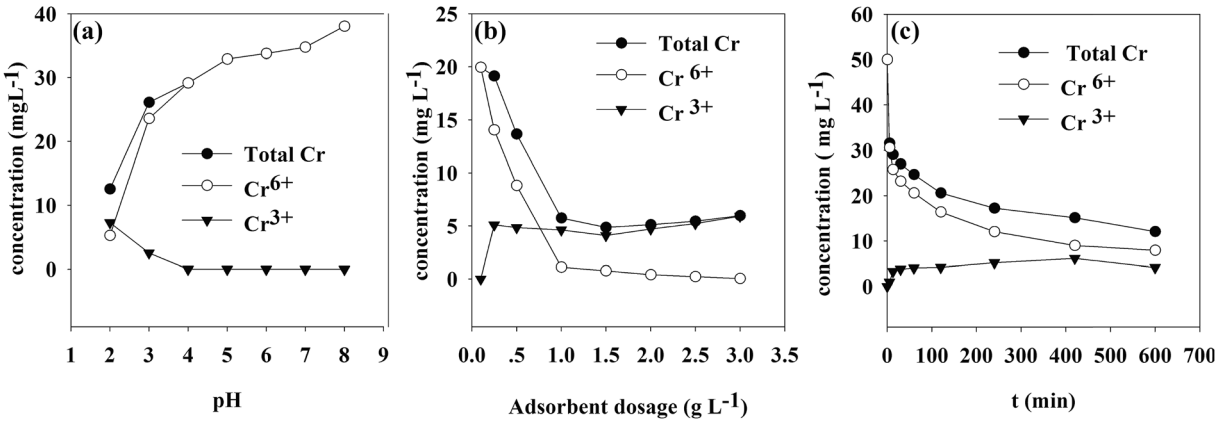

Fig. 12 Concentration of total Cr, Cr(VI), Cr(III) under different parameters (a) pH (b) adsorbent mass (c) contact time.

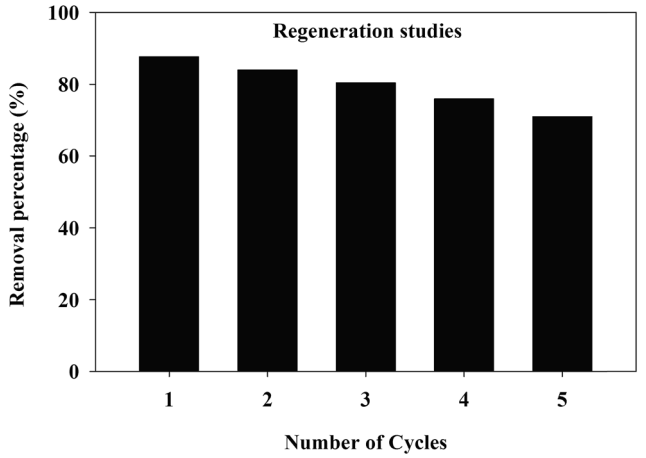

Fig. 13 Desorption–regeneration experiment of the TW/Fe_3O_4 composite for Cr(VI) removal.

The conditions for the adsorption experiments were 50 mg L^{-1} initial concentration of Cr(VI), 40 mL of solution, adsorbent mass 0.1 g, pH 2, temperature 25 °C, 180 rpm for 10 h. When the adsorption process reached equilibrium, 50 mL of NaOH (0.5 mol L^{-1}) was used to desorb the adsorbent for 2 h. The Cr(VI) was determined by a spectrophotometric method. Then, HCl (0.5 mol L^{-1}) was used to regenerate the absorbent.

The Cr(VI) removal rate of the TW/Fe_3O_4 composite after five recycles of desorption–regeneration is shown in Fig. 13 and the removal rate was still higher at more than 70%, indicating the potential recycling of the TW/Fe_3O_4 composite, consistent with the measurement of magnetic hysteresis loops (Fig. 4). Desorption of the Cr(VI) from the TW/Fe_3O_4 composite was favored by weak alkaline conditions[68,69] and HCl could be a choice for the regeneration of adsorbent.[25,67] Therefore, the TW/Fe_3O_4 composite has the potential for regeneration and reusability.

3.10. Proposed mechanisms

The mechanism of Cr(VI) removal is not fully understood and involves many models or steps.[69–76] The adsorption mechanism of Cr(VI) onto the TW/Fe_3O_4 composite is a complicated process and multiple interactions coexist. According to the research of Saha and Orvig,[70] there are four potential mechanisms explaining Cr(VI) sorption by biosorbents: (a) anionic adsorption, (b) adsorption-coupled reduction, (c) anionic and cationic adsorption and (d) reduction and cationic adsorption. According to an analysis of the above results, the mechanism of Cr(VI) sorption by the TW/Fe_3O_4 composite involved adsorption-coupled reduction.

According to the analysis of the FTIR, functional groups (–OH, C=O and C=C, C–O, secondary amine groups, C–N) could participate in the adsorption–reduction process. Herein, the oxygen-containing or nitrogen-containing groups played three functions. First, functional groups could adsorb Cr(VI) through surface complexation, an ion exchange process, *etc.* Second, a functional group could be protonated by the H^+ in the solution, especially the amine functional groups. A protonated functional group could reduce Cr(VI) to Cr(III).[73,74,77] The Cr(III) was confirmed by the analysis of XPS (Fig. 5) and the difference between total Cr and Cr(VI) (Fig. 13). Third, the functional groups could also bind with Cr(III) through surface complexation, an ion-exchange process, *etc.* Thus, functional groups of the TW/Fe_3O_4 composite played an important role during the adsorption–reduction process.

Table 6 The release of Ca^{2+}, Mg^{2+}, Na^+, K^+ during adsorption by a TW/Fe_3O_4 composite at 25 °C[a]

Samples	The net amount of released cations (mequiv. g^{-1})				
	Ca^{2+}	Mg^{2+}	Na^+	K^+	Sum
10 mg L^{-1} to 25 °C	0.0243	−0.0015	−0.0568	0.0448	0.0109
30 mg L^{-1} to 25 °C	0.0264	−0.0003	−0.0505	0.1080	0.0837
50 mg L^{-1} to 25 °C	0.0259	0.0003	−0.0431	0.1714	0.1545

[a] Note: 10 mg L^{-1} to 25 °C means the concentration of Cr(VI) was 10 mg L^{-1} and the operating temperature was 25 °C during the adsorption kinetics experiment.

The ion exchange process is also an important mechanism. The concentrations of Ca^{2+}, Mg^{2+}, Na^+, K^+ in the supernatant were determined and deionized water served as a control. The ion exchange capacities of Ca^{2+}, Mg^{2+}, Na^+, K^+ were calculated and are presented in Table 6. The sum of ion exchange capacity increased when the Cr(VI) was removed by the TW/Fe_3O_4 composite. The ion exchange capacity was higher when the initial concentration of Cr(VI) was higher. Ca^{2+} and K^+ ions participate more in the ion exchange process, consistent with previous studies.[78] The results also confirm the conclusions of the kinetic and isotherm models.

In brief, the adsorption mechanism of Cr(VI) onto the TW/Fe_3O_4 composite referred to physical adsorption, electrostatic interaction, reduction, ion exchange, surface complexation, *etc.*

Meanwhile, Cr(VI) in solution had been adsorbed onto the surface of the adsorbent and then reduced to Cr(III) by a heterogeneous redox process under an acid environment (as shown in eqn (20)). A few Fe^{2+} ions may be oxidized by Cr(VI) although Fe_3O_4 nanoparticles are relatively stable. The reaction process follows eqn (21).[43] The converted Cr(III) was retained by the TW/Fe_3O_4 composite and part of the Cr(III) was released into solution due to electrostatic repulsion. Some portion of the Cr(III) could be adsorbed onto the TW/Fe_3O_4 composite by carbon–oxygen groups or weak acid surface groups.[79–83]

$$HCrO_4^- + 7H^+ + 3e^- \rightarrow Cr^{3+} + 4H_2O \quad (20)$$

$$3Fe^{2+} + CrO_4^{2-} + 4H_2O \rightarrow Cr^{3+} + 3Fe^{3+} + 8OH^- \quad (21)$$

In conclusion, the proposed mechanism of Cr(VI) removal by the TW/Fe_3O_4 composite is as displayed in Fig. 14. The main steps follow: first step, Cr(VI) is adsorbed quickly onto the surface of the TW/Fe_3O_4 composite due to electrostatic attraction (protonated functional groups or positive Fe_3O_4 nanoparticles) or an ion exchange process or surface complexation.

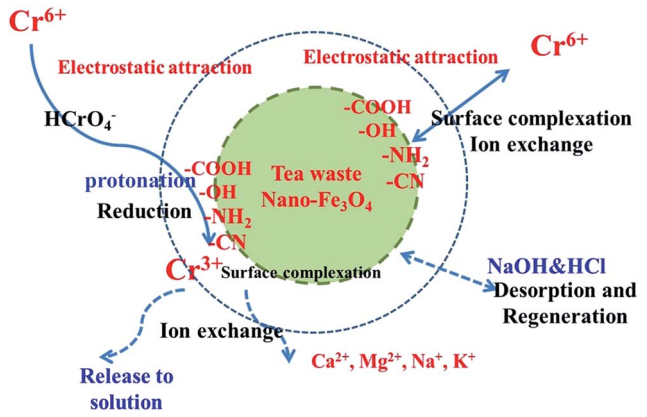

Fig. 14 Proposed mechanism of Cr(VI) removal by the TW/Fe_3O_4 composite.

Second step, some portions of Cr(VI) were reduced to Cr(III). Third step, some Cr(III) was adsorbed onto the surface of the TW/Fe_3O_4 composite through ion exchange or surface complexation. Last step, part of the Cr(III) was released into solution due to electrostatic repulsion. Then, NaOH and HCl acted as the desorption reagent and regeneration reagent, respectively.

4. Conclusions

In this study, a tea waste/nano-Fe_3O_4 composite was facilely prepared and used to remove Cr(VI) from aqueous solution. The maximum removal of Cr(VI) by the TW/Fe_3O_4 composite was observed at pH 2. The adsorption process data was found to best fitted by a pseudo-second-order kinetic model. The maximum adsorption capacity was higher and reached 75.76 mg g^{-1} based on the Langmuir model. Adsorption of hexavalent chromium ions by the TW/Fe_3O_4 composite is spontaneous in nature, endothermic, and results in increased randomness at the adsorbent/adsorbate interface, due to an investigation of the thermodynamics. Desorption and regeneration experiments revealed that the TW/Fe_3O_4 composite had a good potential for recycling. The mechanism of Cr(VI) removal involved an adsorption–reduction process, referring to physical adsorption, electrostatic interaction, reduction, ion exchange, surface complexation, *etc.* 70% of the Cr(VI) was reduced to Cr(III) in this investigation. Therefore, the TW/Fe_3O_4 composite could be applied as a novel adsorbent for Cr(VI) removal from industrial wastewater.

List of symbols

b_T	Temkin isotherm constant (J mol^{-1})
C_0	Initial Cr(VI) concentration (mg L^{-1})
C_e	Cr(VI) concentration in solution at equilibrium (mg L^{-1})
C_t	Concentration of Cr(VI) at t time (mg L^{-1})
K_f	Freundlich isotherm constant (mg g^{-1}) (mg $L^{-1})^{-1}$
k_1	Pseudo-first-order rate constant ($L\ min^{-1}$)
k_2	Pseudo-second-order rate constant (g mg^{-1} min^{-1})
k_{id}	Intraparticle diffusion rate constant (mg g^{-1} $min^{-0.5}$)
K_0	Apparent equilibrium constant
m	Amount of adsorbent (TW/Fe_3O_4) composite (g)
q_t	Adsorption capacities of Cr(VI) ions at time t (mg g^{-1})
q_e	Adsorption capacities of Cr(VI) ions at equilibrium time (mg g^{-1})
q_{max}	The maximum adsorption capacity based on Langmuir model (mg g^{-1})
q_m	Maximum adsorption capacity (mg g^{-1}) in D–R model
R	Ideal gas constant, 8.314 J mol^{-1} K^{-1}
R^2	Coefficient of determination
R_L	Dimensionless separation factor
T	Kelvin temperature (K)
V	Volume of Cr(VI) solution (L)
$1/n$	The heterogeneity of the sorption sites and an indicator of isotherm nonlinearity
ΔG	Gibbs free energy (kJ mol^{-1})
ΔH	Enthalpy (kJ mol^{-1})
ΔS	Entropy (J mol^{-1} K^{-1})
ε	Dubinin–Radushkevich isotherm constant
α	The initial adsorption coefficient in Evolich model (mg g^{-1} min^{-1})
β	The desorption coefficient in Evolich model (g mg^{-1})
β_{D-R}	Dubinin–Radushkevich isotherm constant (mol^2 kJ^{-2})

Acknowledgements

This study was financially supported by Natural Science Foundation of China (No. 51609001), National Major Water Project (No. 2015ZX07103007) and Anhui Agricultural University Youth Fund Project (No. 2014zr004, jz2015-23).

References

1 D. Mohan and C. U. Pittman Jr, *J. Hazard. Mater.*, 2006, **137**, 762–811.
2 J. Kotaś and Z. Stasicka, *Environ. Pollut.*, 2000, **107**, 263–283.
3 M. Owlad, M. K. Aroua, W. D. W. Ashri and S. Baroutian, *Water, Air, Soil Pollut.*, 2009, **200**, 59–77.
4 Y. Liu, C. Luo, G. Cui and S. Yan, *RSC Adv.*, 2015, **5**, 54156–54164.
5 T. Khan, M. H. Isa, M. R. Ul Mustafa, H. Yeek-Chia, L. Baloo, T. S. Binti Abd Manan and M. O. Saeed, *RSC Adv.*, 2016, **6**, 56365–56374.
6 D. Ding, X. Ma, W. Shi, Z. Lei and Z. Zhang, *RSC Adv.*, 2016, **6**, 74675–74682.
7 D. Sud, G. Mahajan and M. P. Kaur, *Bioresour. Technol.*, 2008, **99**, 6017–6027.
8 M. M. Zhang, Y. G. Liu, T. T. Li, W. H. Xu, B. H. Zheng, X. F. Tan, H. Wang, Y. M. Guo, F. Y. Guo and S. F. Wang, *RSC Adv.*, 2015, **5**, 46955–46964.
9 B. Amarasinghe and R. Williams, *Chem. Eng. J.*, 2007, **132**, 299–309.
10 S. Çay, A. Uyanık and A. Özaşık, *Sep. Purif. Technol.*, 2004, **38**, 273–280.

11 H. D. Utomo and K. A. Hunter, *Environ. Technol.*, 2006, **27**, 25–32.
12 S. Wan, Z. Ma, Y. Xue, M. Ma, S. Xu, L. Qian and Q. Zhang, *Ind. Eng. Chem. Res.*, 2014, **53**, 3629–3635.
13 S. S. Ahluwalia and D. Goyal, *Eng. Life Sci.*, 2005, **5**, 158–162.
14 E. Malkoc and Y. Nuhoglu, *J. Hazard. Mater.*, 2005, **127**, 120–128.
15 E. Malkoc and Y. Nuhoglu, *J. Hazard. Mater.*, 2006, **135**, 328–336.
16 E. Malkoc and Y. Nuhoglu, *Chem. Eng. Sci.*, 2006, **61**, 4363–4372.
17 E. Malkoc and Y. Nuhoglu, *Sep. Purif. Technol.*, 2007, **54**, 291–298.
18 D. Chen, Y. Li, J. Zhang, J. Zhou, Y. Guo and H. Liu, *Chem. Eng. J.*, 2012, **185–186**, 120–126.
19 J. Liu, Z. Zhao, G. Jiang and C. Ren, *Environ. Sci. Technol.*, 2008, **42**, 6949–6954.
20 S. Nethaji, A. Sivasamy and A. Mandal, *Bioresour. Technol.*, 2013, **134**, 94–100.
21 C. Su, *J. Hazard. Mater.*, 2016, **32**, 48–84.
22 P. Panneerselvam, N. Morad and K. A. Tan, *J. Hazard. Mater.*, 2011, **186**, 160–168.
23 A. A. Babaev and T. S. Salimov, *Desalin. Water Treat.*, 2015, **57**, 1–13.
24 Y. S. Kang, S. Risbud, J. F. Rabolt and P. Stroeve, *Chem. Mater.*, 1996, **8**, 2209–2211.
25 C. Ding, W. Cheng, Y. Sun and X. Wang, *J. Hazard. Mater.*, 2015, **295**, 127–137.
26 B. Chen, Z. Chen and S. Lv, *Bioresour. Technol.*, 2011, **102**, 716–723.
27 E. E. Özbaş, A. Öngen and C. E. Gökçe, *Desalin. Water Treat.*, 2013, **51**, 7523–7535.
28 H. Eroğlu, S. Yapici, Ç. Nuhoğlu and E. Varoğlu, *J. Hazard. Mater.*, 2009, **163**, 607–617.
29 Q. Zhang, X. Han and B. Tang, *RSC Adv.*, 2013, **3**, 9924–9931.
30 S. Ni, X. Wang, G. Zhou, F. Yang, J. Wang, Q. Wang and D. He, *Mater. Lett.*, 2009, **63**, 2701–2703.
31 H. Gu, S. B. Rapole, J. Sharma, Y. Huang, D. Cao, H. A. Colorado, Z. Luo, N. Haldolaarachchige, D. P. Young, B. Walters, S. Wei and Z. Guo, *RSC Adv.*, 2012, **2**, 11007–11018.
32 N. Fiol, C. Escudero and I. Villaescusa, *Bioresour. Technol.*, 2008, **99**, 5030–5036.
33 W. Cheng, C. Ding, X. Wang, Z. Wu, Y. Sun, S. Yu, T. Hayat and X. Wang, *Chem. Eng. J.*, 2016, **293**, 311–318.
34 G. Yang, L. Tang, Y. Cai, G. Zeng, P. Guo, G. Chen, Y. Zhou, J. Tang, J. Chen and W. Xiong, *RSC Adv.*, 2014, **4**, 58362–58371.
35 E. J. Kim, S. Park, H. J. Hong, Y. E. Choi and J. W. Yang, *Bioresour. Technol.*, 2011, **102**, 11155–11160.
36 T. Wang, L. Zhang, C. Li, W. Yang, T. Song, C. Tang, Y. Meng, S. Dai, H. Wang and L. Chai, *Environ. Sci. Technol.*, 2015, **49**, 5654–5662.
37 X. Yao, S. Deng, R. Wu, S. Hong, B. Wang, J. Huang, Y. Wang and G. Yu, *RSC Adv.*, 2016, **6**, 8797–8805.
38 D. Kołodyńska, R. Wnętrzak, J. Leahy, M. Hayes, W. Kwapiński and Z. Hubicki, *Chem. Eng. J.*, 2012, **197**, 295–305.
39 X. F. Sun, M. Yue, X. W. Liu, S. G. Wang, B. Y. Gao and X. M. Li, *Water Res.*, 2010, **44**, 2517–2524.
40 J. Zhang and P. Zheng, *RSC Adv.*, 2015, **5**, 17768–17774.
41 H. L. Ma, Y. Zhang, Q. H. Hu, D. Yan, Z. Z. Yu and M. Zhai, *J. Mater. Chem.*, 2012, **22**, 5914–5916.
42 P. Yuan, M. Fan, D. Yang, P. He, D. Liu, A. Yuan, J. Zhu and T. Chen, *J. Hazard. Mater.*, 2009, **166**, 821–829.
43 J. Hu, I. M. C. Lo and G. Chen, *Water Sci. Technol.*, 2004, **50**, 139–146.
44 S. Chen, Q. Yue, B. Gao and X. Xing, *J. Colloid Interface Sci.*, 2010, **349**, 256–264.
45 M. Barkat, D. Nibou, S. Chegrouche and A. Mellah, *Chen. Eng. Process*, 2009, **48**, 38–47.
46 Y. S. Ho, *J. Hazard. Mater.*, 2006, **37**, 681–689.
47 Y. S. Ho and G. Mckay, *Process Biochem.*, 1999, **34**, 451–465.
48 S. H. Hasan, K. K. Singh, O. Prakash, M. Talat and Y. S. Ho, *J. Hazard. Mater.*, 2008, **152**, 356–365.
49 Y. Sun, C. Ding, W. Cheng and X. Wang, *J. Hazard. Mater.*, 2014, **280**, 399–408.
50 C. Dan, L. Yang, Z. Jia, W. Li, J. Zhou, S. Li and G. Qian, *J. Hazard. Mater.*, 2012, **243**, 152–160.
51 S. H. Chien and W. R. Clayton, *Soil Sci. Soc. Am. J.*, 1980, **44**, 265–268.
52 D. Park, Y. S. Yun, H. W. Lee and J. M. Park, *Bioresour. Technol.*, 2008, **99**, 1141–1147.
53 I. S. Ng, X. Wu, X. Yang, Y. Xie, Y. Lu and C. Chen, *Bioresour. Technol.*, 2013, **145**, 297–301.
54 I. Langmuir, *J. Am. Chem. Soc.*, 1917, **38**, 102–105.
55 H. M. F. Freundlich, *J. Phys. Chem.*, 1906, **57**, 385–471.
56 M. Temkin and V. Pyzhev, *Acta Physicochim. URSS*, 1940, **12**, 217–222.
57 B. Kavitha and D. Sarala Thambavani, *RSC Adv.*, 2016, **6**, 5837–5847.
58 E. Nakkeeran, S. Rangabhashiyam, M. S. G. Nandagopal and N. Selvaraju, *Desalin. Water Treat.*, 2016, **57**, 1–14.
59 S. Rangabhashiyam, E. Nakkeeran, N. Anu and N. Selvaraju, *Res. Chem. Intermed.*, 2015, **41**, 1–20.
60 S. Rangabhashiyam and N. Selvaraju, *J. Mol. Liq.*, 2015, **209**, 487–497.
61 T. W. Weber and R. K. Chakravorti, *AIChE J.*, 1974, **20**, 228–238.
62 M. Xu, Y. Zhang, Z. Zhang, Y. Shen, M. Zhao and G. Pan, *Chem. Eng. J.*, 2011, **168**, 737–745.
63 G. Mckay, H. S. Blair and J. R. Gardner, *J. Appl. Polym. Sci.*, 1982, **27**, 3043–3057.
64 A. H. Chen, S. C. Liu, C. Y. Chen and C. Y. Chen, *J. Hazard. Mater.*, 2008, **154**, 184–191.
65 X. Chang, M. Li, Q. Liu, Q. Liu and J. Yao, *RSC Adv.*, 2016, **6**, 46879–46888.
66 A. A. Khan and R. P. Singh, *Colloids Surf.*, 1987, **24**, 33–42.
67 T. Lin, F. Yan, Y. Pang, G. Zeng, J. Wang, Y. Zhou, Y. Deng, G. Yang, C. Ye and J. Chen, *Chem. Eng. J.*, 2014, **254**, 302–312.
68 C. Gan, Y. Liu, X. Tan, S. Wang, G. Zeng, B. Zheng, T. Li, Z. Jiang and W. Liu, *RSC Adv.*, 2015, **5**, 35107–35115.

69 H. Wang, X. Xu, Z. Ren and B. Gao, *RSC Adv.*, 2016, **6**, 47237–47248.
70 B. Saha and C. Orvig, *Coord. Chem. Rev.*, 2010, **254**, 2959–2972.
71 D. Park, Y. S. Yun, H. J. Ji and J. M. Park, *Water Res.*, 2005, **39**, 533–540.
72 X. Huang, Y. Liu, S. Liu, X. Tan, Y. Ding, G. Zeng, Y. Zhou, M. Zhang, S. Wang and B. Zheng, *RSC Adv.*, 2016, **6**, 94–104.
73 Z. Lei, S. Zhai, J. Lv, Y. Fan, Q. An and Z. Xiao, *RSC Adv.*, 2015, **5**, 77932–77941.
74 M.-r. Shang, Y.-g. Liu, S.-b. Liu, G.-m. Zeng, X.-f. Tan, L.-h. Jiang, X.-x. Huang, Y. Ding, Y.-m. Guo and S.-f. Wang, *RSC Adv.*, 2016, **6**, 85202–85212.
75 F. Gao, H. Gu, H. Wang, X. Wang, B. Xiang and Z. Guo, *RSC Adv.*, 2015, **5**, 60208–60219.
76 Y. Ma, W. J. Liu, N. Zhang, Y. S. Li, H. Jiang and G. P. Sheng, *Bioresour. Technol.*, 2014, **169**, 403–408.
77 D. Zhao, X. Gao, C. Wu, R. Xie, S. Feng and C. Chen, *Appl. Surf. Sci.*, 2016, **384**, 1–9.
78 Q. H. Shen, T. T. Zhi, L. H. Cheng, X. H. Xu and H. L. Chen, *Chem. Eng. J.*, 2013, **228**, 993–1002.
79 T. Cordero, J. Rodriguez-Mirasol, N. Tancredi, J. Piriz, G. Vivo and J. Rodriguez, *Ind. Eng. Chem. Res.*, 2002, **41**, 6042–6048.
80 S. Wan, Z. Ma, Y. Xue, M. Ma, S. Xu, L. Qian and Q. Zhang, *Ind. Eng. Chem. Res.*, 2014, **53**, 3629–3635.
81 J. Rivera-Utrilla and M. Sánchez-Polo, *Water Res.*, 2003, **37**, 3335–3340.
82 Y. Nakano, K. Takeshita and T. Tsutsumi, *Water Res.*, 2001, **35**, 496–500.
83 Z. Lu, Y. Liu, S. Liu, Y. Yin, G. Zeng, X. Tan, H. Xi, X. Hu, L. Jiang and D. Yang, *Bioresour. Technol.*, 2016, **218**, 351–359.